Operational Reliability Modeling and Assessment of Battery Energy Storage Based on Lithium-ion Battery Lifetime Degradation

Lin Cheng, *Senior Member*, *IEEE*, Yuxiang Wan, *Student Member*, *IEEE*, Yanglin Zhou, *Member*, *IEEE*, and David Wenzhong Gao, *Fellow*, *IEEE*

***Abstract*—Battery energy storage (BES) systems can effectively meet the diversified needs of power system dispatching and assist in renewable energy integration. The reliability of energy storage is essential to ensure the operational safety of the power grid. However, BES systems are composed of battery cells. This suggests that BES performance depends not only on the configuration but also on the operating state over different lifetime durations. The lack of safety and reliability is the main bottleneck preventing widespread applications of BES systems. Therefore, a reliability assessment algorithm and a weak-link analytical method for BES systems are proposed while considering battery lifetime degradation. Firstly, a novel lithium-ion battery model is proposed to identify the degradation rate of solid electrolyte interphase film formation and capacity plummeting. The impacts of different operating conditions are considered in stress factor models. Then, a reliability assessment algorithm for a BES system is introduced based on a universal generating function. An innovative weak-link analytical method based on the reliability importance index is proposed that combines the evaluation results of state-oriented and state-change-oriented indexes through an entropy weight method. The model, algorithm, indexes, and the usefulness are demonstrated in case studies based on aging test data and actual bus operating data. The results demonstrate the effects of the battery status and working conditions on BES reliability. Weak-link analysis is also used to assist BES systems in avoiding short-board batteries to achieve long lifetimes and efficient operation.**

***Index Terms*—Battery energy storage, lifetime degradation, operational reliability, capacity plummeting, weak-link analysis.**

NOMENCLATURE

A. Sets and Indices

Ψ	State of health (SOH) set of battery cells
i, j, k, m	Subscripts representing the i^{th} charging cycle, the j^{th} SOH grade, the number of the battery, and the m^{th} reliability index
ref	Subscript representing the reference value of different variables
z	Power law factor

B. Variables

ω	Required SOH threshold
C_{cycle}	Number of cycles
e_m, dis_m, w_m	Entropy, Laplace distance, and information entropy redundancy of the m^{th} index
p_j, p'_j, p''_j	Probability in the j^{th} SOH grade
R_{BES}, E_{BES}	Reliability and expected SOHs of BES
t, τ, υ, T	Operation time, average state of charge (SOC), charge/discharge depth, average temperature, and operation time
$I_{k,m}$, $I'_{k,m}$	The m^{th} index value of the k^{th} cell and the corresponding normalized value

C. Parameters

β_{sei}, β_{cps}	Coefficients for solid electrolyte interphase (SEI) model and the capacity plummeting model
κ, κ_1, κ_2	Correction factors
α_{sei}, α_{sds}	Portion of capacity consumed irreversibly for SEI formation and the consumed capacity during the steady degradation stage
d_{cyc}	Linear degradation rate
d_{sei}, d_{sds}, d_{cps}	Degradation rates in SEI formation stage, steady degradation stage, and capacity plummeting stage
G_j, G_{j1}, G_{j2}	The j^{th}, j_1^{th}, j_2^{th} SOH grades
l_T, l_t, l_τ, l_υ	Coefficients of temperature stress, time stress , SOC stress, and depth of discharge (DOD) stress

Manuscript received: March 23, 2021; revised: June 26, 2021; accepted: September 7, 2021. Date of CrossCheck: September 7, 2021. Date of online publication: November 24, 2021.

This work was supported by the National Key R&D Program of China (No. 2018YFC1902200) and the National Natural Science Foundation of China (No. 51777105).

L. Cheng, Y. Wan (corresponding author), and Y. Zhou are with the State Key Laboratory of Control and Simulation of Power System and Generation Equipment, Department of Electrical Engineering, Tsinghua University, Beijing, China (e-mail: chenglin@tsinghua. edu. cn; wyx17@mails. tsinghua. edu. cn; zhouylstu@mail.tsinghua.edu.cn).

D. W. Gao is with the Department of Electrical and Computer Engineering, University of Denver, Denver, USA (e-mail: wenzhong.gao@foxmail.com).

DOI: 10.35833/MPCE.2021.000197

L_c	Consumed capacity
M	Number of SOH grades
n	A full/half cycle
N	Total number of equivalent cycles
N_p	Number of parallel branches
N_s	Number of cells in series
SOH_{G_j}	SOH level of the j^{th} grade
D. Functions	
$\Omega(\cdot)$	Universal generated function
$d_L^{cyc}(\cdot)$	Capacity degradation in one cycle
$d_c(\cdot)$, $d_t(\cdot)$	Cycle and calendar aging rates
$f(\cdot)$	Symbolic multiplier
$F(\cdot)$, $F'(\cdot)$	Original and modified cumulative distribution functions
$S_t(\cdot)$, $S_\tau(\cdot)$, $S_T(\cdot)$, $S_v(\cdot)$	Stress factor models of time, average SOC, average temperature, and DOD
$U_R(\cdot)$	Universal generating function

I. Introduction

With its distinct advantages of rapid power response, high energy density, and flexible deployment, battery energy storage (BES) plays an important role in applications such as frequency regulation, peak shaving, renewable energy fluctuation suppression, and economic dispatch [1]-[3]. In addition, with the rapid development of new loads such as electric vehicles (EVs) and internet data centers, recycling has become an urgent need for numerous decommissioned lithium-ion batteries [4]. Grid applications of decommissioned BES systems represent promising solutions [5]. However, the cycle life of a BES composed of large battery cells is severely reduced. Inadequate reliability is a major obstacle to the applications of BES systems. Evaluating and improving the reliability of BES have thus become focal issues [6], [7].

In the case of complex systems with large battery cells, the level of reliability of energy storage is closely related to the battery state. Because of the complex electrochemical reactions involved when batteries are used, unavoidable differences exist between the cells, which are further amplified once the batteries are grouped [7], [8]. The short-board effect involves battery cells with weaker performance being overcharged or overdischarged. Therefore, analyzing and evaluating the reliability of energy storage systems under operating conditions represent the main obstacles to achieving long-life and efficient operation of energy storage systems. In addition, the effects of various factors such as battery parameter differences, operating conditions, and the environment must also be considered [9].

The operational reliability model of battery cells is a critical premise in achieving an operational reliability assessment of the BES. The state of health (SOH) has been mostly used to measure battery reliability in recent studies [9]-[11]. The capacity degradation models of lithium-ion batteries can be categorized into empirical [12]-[14], electrochemical mechanism [15]-[17], and semi-empirical models [18], [19]. Of these, the empirical models are aimed at specific working conditions or specific use of lithium-ion batteries using a fitting function to obtain the relationship between the battery capacity degradation and certain working conditions in the aging tests. For instance, [11] and [12] used an exponential function and a polynomial function, respectively, to fit the battery degradation process. The generalizability of this type of model is poor, which leads to the need for a long-term cyclic aging test to obtain an accurate model [14]. In addition, the electrochemical mechanism model must combine detailed battery aging mechanism analyses and the battery working conditions, where combining the charging/discharging process with the internal electrochemical reactions of the battery such as the lithium-ion concentration [17] is difficult. To address these difficulties, a semi-empirical model that effectively combines test data with operating data has been proposed in recent research. Reference [18] analyzed the formation mechanism of a solid electrolyte interphase (SEI) film and established stress factor models to reflect the fatigue accumulation process resulting from charging and discharging cycles. In this model, a statistical fitting method was used to determine the functional relationship between battery degradation, temperature, and state of charge (SOC). However, the aforementioned studies all utilized 80% of the rated maximum capacity as the standard for battery decommissioning. These models are thus not applicable to battery degradation processes below 80% SOH.

In fact, few studies have been conducted on lifetime capacity degradation models of lithium-ion batteries. Most adopted simple data fitting methods that are used in the degradation process below 80% SOH, and these model parameters usually do not correspond to actual physical meanings. For example, in [20], linear extrapolation was directly carried out using limited cycle test data to estimate the secondary life of batteries. A lifetime aging model was proposed for battery life estimation in [21], in which the degradation process was expressed as a function of time and charging flow. Reference [22] utilized multi-Gaussian functions to fit lifetime capacity degradation. However, the battery degradation process during the entire lifetime was not linear. In the early stage, SEI formation required the consumption of active lithium-ions, resulting in a greater degradation rate [19]. Battery capacity plummeting in the decommissioning stage is rarely considered in existing research and is mainly caused by lithium evolution from the negative electrode [23], [24]. Both characteristics should be reflected in the parameters of lifetime degradation models.

In addition, analyzing and evaluating the BES reliability must consider the effects of various factors such as battery parameter differences, operating conditions, and the environment [9]. Commonly used reliability assessment methods such as fault tree analysis [25] and the Markov model [26], [27] usually divide a BES system into several subsystems such as the battery pack, balancing circuit, and converter [26]. However, because of the complex electrochemical reactions involved in the use of batteries, unavoidable differenc-

es exist between the cells, which are further amplified once the batteries are grouped [28]. The failure rates with the aforementioned method are still the statistical average value, which ignore the health status of the battery cells, and are more suitable for system design on a long time scale. Fortunately, the universal generating function (UGF) method is very effective for analyzing the reliability of multistate systems [8]-[10], [29]. References [8] and [9] defined the reliability failure of a battery cell as occurring when its probabilistic capacity is less than 80% of the rated capacity. In these studies, the relationship between the battery degradation model and system reliability was further established using the UGF method. The influence of redundant backup strategies and topologies on the reliability of the BES was analyzed. However, the ultimate goal of reliability evaluation was to identify weak links and analyze the effects of different cell reliability changes on BES reliability. The research on the precise identification of weak links as well as the corresponding measurement indexes is essentially absent in the current algorithm, which is significant for improving BES reliability.

Motivated by the above background, this paper proposes a novel reliability model and an assessment algorithm for BES. A condition-dependent model for lithium-ion battery lifetime degradation is established, as conventional models are not applicable for capacity assessment of batteries below 80% SOH. The universal generation function based method is then considered necessary for BES reliability evaluation. New reliability indexes for weak-link analysis are also proposed in this paper. The proposed model, algorithm, and indexes are deployed in a BES system composed of differentiated batteries. These case studies indicate better fitting effects and more accurate reliability assessment results of the proposed model while considering the nonlinear degradation rate affected by various operating conditions. The main contributions of this paper are as follows.

1) A semi-empirical lifetime degradation model of lithium-ion batteries is proposed considering the formation of the SEI and battery capacity plummeting, where the threshold of the reliability evaluation can thus be greatly extended. This model is not only accurate in its analyses of experimental data but also suitable for different stress factor analyses under actual operating conditions.

2) An improved reliability algorithm for BES is proposed that consists of a reliability evaluation and weak-link analysis. The factors such as operating conditions, battery health, and ambient temperature can be included in the analysis, making it particularly suitable for operational reliability assessment of BESs with differentiated batteries.

3) State-oriented and state-change-oriented indexes are developed to compare the influence of different battery states on BES reliability. A reliability importance (RI) index based on an entropy weight method is proposed to identify the weak links of BES systems more accurately and objectively.

The remainder of this paper is organized as follows. Section II introduces the modeling of lithium-ion battery lifetime degradation. Section III discusses the reliability assessment and weak component analysis of BES. Section IV presents the main reliability assessment algorithm. Case studies are presented in Section V. Finally, conclusions and future work are summarized in Section VI.

II. Modeling of Lithium-ion Battery Lifetime Degradation

Estimating the battery SOH before evaluating the overall reliability of a BES system is critical. This section focuses on the structure of a lifetime degradation model of lithium-ion batteries and the corresponding stress factor model.

A. Lifetime Degradation Model of Lithium-ion Batteries

The degradation rate of lithium-ion batteries is typically non-linear during their lifetimes. Aging tests show that the degradation rate is much higher in the early and decommissioning stages than in the steady degradation state (SDS) stages [30]. Some studies have expressed the actual capacity degradation in one cycle as a function of the consumed capacity and linear degradation rate d_{cyc} [18], [31]. Note that L_{c} is a normalized quantity between 0 and 1. If the battery life is defined as the time required for the battery to provide only 20% of the rated capacity, then $L_{\mathrm{c}}=80\%$.

$$\frac{\mathrm{d}L_{\mathrm{c}}}{\mathrm{d}C_{cycle}}=d_{\mathrm{L}}^{\mathrm{cyc}}\left(L_{\mathrm{c}},d_{\mathrm{cyc}}\right)\quad L_{\mathrm{c}}\in\left[0,100\%\right] \tag{1}$$

In the early and SDS stages, the existing research indicates that the steady degradation rate is proportional to the number of the remaining active lithium-ions [32]. This means that the lower the amount of remaining lithium-ions, the slower the degradation rate. The degradation process appears to be initially fast and then slow. As the battery capacity plummets during the decommissioning stage, the number of active lithium-ions is significantly reduced due to lithium evolution in the negative electrode, which leads to an increased degradation rate [23]. Thus, the degradation rate can be assumed to be inversely proportional to the number of active lithium-ions remaining in the battery. This relationship can be expressed as:

$$d_{\mathrm{L}}^{\mathrm{cyc}}\left(L_{\mathrm{c}},d_{\mathrm{cyc}}\right)=\begin{cases}\left(1-L_{\mathrm{c}}\right)d_{\mathrm{cyc}} & \text{early/SDS}\\ L_{\mathrm{c}}d_{\mathrm{cyc}} & \text{capacity plummeting}\end{cases} \tag{2}$$

The basic battery degradation life is obtained by integrating the equation with respect to L_{c}:

$$L_{\mathrm{c}}=\begin{cases}1-\kappa_1\mathrm{e}^{-d_{\mathrm{L}}} & \text{early/SDS}\\ 1-\left(1-\kappa_2\mathrm{e}^{d_{\mathrm{L}}}\right) & \text{capacity plummeting}\end{cases} \tag{3}$$

In addition, it should be noted that the fast aging rate at the early stage is caused by various factors, the major one of which is SEI formation [33]. Once a stable film is formed, the battery is in the normal degradation stage. Experimental results from the aforementioned paper show that α_{sei} is between 3% and 8%, as determined by the electrode material and operating conditions. Let α_{sds} be the consumed capacity during the SDS, which means that the battery capacity starts to plummet, whereas the consumed capacity portion is $\left(\alpha_{\mathrm{sei}}+\right.$

α_{sds}). The existing research generally indicates that lithium-ion batteries enter the decommissioning stage at approximately 80% SOH, i.e., the capacity plummeting stage. The specified threshold varies for different batteries.

Accordingly, the capacity degradation of the battery can be divided into three parts: the SEI formation stage with a degradation rate d_{sei}, the SDS with a linearized rate d_{sds}, and the capacity plummeting stage with a different rate d_{cps} inversely proportional to the battery life. The battery life model is expressed as a three-exponential function:

$$L_{\mathrm{c}} = 1 - \alpha_{\mathrm{sei}} \mathrm{e}^{-d_{\mathrm{sei}}} - \alpha_{\mathrm{sds}} \mathrm{e}^{-d_{\mathrm{sds}}} - \left(1 - \alpha_{\mathrm{sei}} - \alpha_{\mathrm{sds}}\right)\left(1 - \kappa \mathrm{e}^{d_{\mathrm{cps}}}\right) \quad (4)$$

Because the degradation during SEI formation and capacity plummeting stages is also nearly linear, we can assume that d_{sei} and d_{cps} are proportional to d_{sds}. Then, (4) and the battery SOH can be expressed as:

$$\begin{cases} L_{\mathrm{c}} = 1 - \alpha_{\mathrm{sei}} \mathrm{e}^{-\beta_{\mathrm{sei}} d_{\mathrm{sds}}} - \alpha_{\mathrm{sds}} \mathrm{e}^{-d_{\mathrm{sds}}} - \left(1 - \alpha_{\mathrm{sei}} - \alpha_{\mathrm{sds}}\right)\left(1 - \kappa \mathrm{e}^{\beta_{\mathrm{cps}} d_{\mathrm{sds}}}\right) \\ SOH = \alpha_{\mathrm{sei}} \mathrm{e}^{-\beta_{\mathrm{sei}} d_{\mathrm{sds}}} + \alpha_{\mathrm{sds}} \mathrm{e}^{-d_{\mathrm{sds}}} + \left(1 - \alpha_{\mathrm{sei}} - \alpha_{\mathrm{sds}}\right)\left(1 - \kappa \mathrm{e}^{\beta_{\mathrm{cps}} d_{\mathrm{sds}}}\right) \end{cases} \quad (5)$$

Parameter identification reveals that the first part, namely, $\alpha_{\mathrm{sei}} \mathrm{e}^{-\beta_{\mathrm{sei}} d_{\mathrm{sds}}}$, dominates during SEI formation, the degradation rate is relatively high, and the degradation function is downward convex. In the SDS, the dominant part is $\alpha_{\mathrm{sds}} \mathrm{e}^{-d_{\mathrm{sds}}}$, which operates at a slower rate. In the capacity plummeting stage, function determination represents the third part $\left(1 - \alpha_{\mathrm{sei}} - \alpha_{\mathrm{sds}}\right)\left(1 - \kappa \mathrm{e}^{\beta_{\mathrm{cps}} d_{\mathrm{sds}}}\right)$, whereas the capacity degradation accelerates in an upward convex direction.

Based on the aforementioned model, the main objective is to obtain the linearized degradation rate d_{sds}, which depends on the battery operating conditions, including various factors such as the SOC level, depth of discharge (DOD), operating temperature, and operating duration. The degradation process of the lithium-ion battery capacity can be decomposed into calendar aging and cyclic aging. Calendar aging of the battery refers to the capacity degradation that occurs over time, and its degradation rate is affected by the average temperature and average SOC over time. Cycle aging reflects the degradation between charging and discharging, the rate of which is determined by the DOD, SOC, and average temperature of each cycle [14]. The total linear degradation rate is expressed as (6), where $\bar{\tau}$ and $\bar{T}$ are the average SOC and temperature of the total operating time.

$$d_{\mathrm{sds}}\left(t, \tau, \upsilon, T\right) = d_{\mathrm{t}}\left(t, \bar{\tau}, \bar{T}\right) + \sum_{i=1}^{N} n_i d_{\mathrm{c}}\left(\tau_i, \upsilon_i, T_i\right) \quad (6)$$

The parameters $\left(t, \tau, \upsilon, T\right)$ can be obtained using the rainflow cycle-counting algorithm. For the cycle aging test, the operating conditions of each cycle are nearly the same. Thus, the cycle degradation rate can be simplified as:

$$d_{\mathrm{sds}}\left(t, \tau, \upsilon, T\right) = N d_{\mathrm{L}}^{\mathrm{cyc}} = N\left(d_{\mathrm{t}}\left(t_i, \tau_i, T_i\right) + d_{\mathrm{c}}\left(\tau_i, \upsilon_i, T_i\right)\right) \quad (7)$$

Then, (5) can be rewritten as:

$$SOH = \alpha_{\mathrm{sei}} \mathrm{e}^{-N\beta_{\mathrm{sei}} d_{\mathrm{L}}^{\mathrm{cyc}}} + \alpha_{\mathrm{sds}} \mathrm{e}^{-N d_{\mathrm{L}}^{\mathrm{cyc}}} + \left(1 - \alpha_{\mathrm{sei}} - \alpha_{\mathrm{sds}}\right)\left(1 - \kappa \mathrm{e}^{N\beta_{\mathrm{cps}} d_{\mathrm{L}}^{\mathrm{cyc}}}\right) \quad (8)$$

We can then use the particle swarm algorithm to fit the values of the parameters $\alpha_{\mathrm{sei}}, \beta_{\mathrm{sei}}, \alpha_{\mathrm{sds}}, \beta_{\mathrm{cps}}, \kappa$, and d_{c} through 1stopt software.

B. Stress Factor Models

Stress factor models of lithium-ion batteries have been extensively studied [18], [32], [34]. The calendar and cycle aging rates can be formulated as:

$$\begin{cases} d_{\mathrm{t}}\left(t, \bar{\tau}, \bar{T}\right) = S_t(t) S_\tau(\bar{\tau}) S_T\left(\bar{T}\right) \\ d_{\mathrm{c}}\left(\tau_i, \upsilon_i, T_i\right) = S_\tau\left(\tau_i\right) S_\upsilon\left(\upsilon_i\right) S_T\left(T_i\right) \end{cases} \quad (9)$$

The stress factor models of calendar aging can be calculated by the average value over the entire operational period, whereas those of cycle aging are the parameters of a specified cycle.

1) Temperature stress factor model: the temperature effect is usually analyzed using the Arrhenius equation. A more detailed description of the derivation method can be found in [35]. This paper utilizes the expression as:

$$S_T(T) = \mathrm{e}^{l_T\left(T - T_{\mathrm{ref}}\right)\frac{T_{\mathrm{ref}}}{273 + T}} \quad (10)$$

Note that this model is applicable above 15 °C because the relationship between the degradation rate and temperature derived from the Arrhenius equation is not applicable at low temperatures, which may accelerate the aging process.

2) Time stress factor model: calendar aging is affected by the duration of operation or storage. This effect can be modeled using a simple linear function [18]:

$$S_t = l_t t \quad (11)$$

3) SOC stress factor model: this paper adopts an exponential function to model the SOC stress factor [32].

$$S_\tau = \mathrm{e}^{l_\tau\left(\tau - \tau_{\mathrm{ref}}\right)} \quad (12)$$

4) DOD stress factor model: the DOD stress factor model has been well studied in recent years and is usually different from the electrode material of lithium-ion batteries. The nonlinear DOD stress factor model usually includes both exponential [32] and quadratic [33] models. This paper adopts the DOD stress factor model from [18], which is suitable for $LiMn_2O_4$ batteries:

$$S_\upsilon(\upsilon) = \frac{1}{l_{\upsilon 1} \delta^{l_{\upsilon 2}} + l_{\upsilon 3}} \quad (13)$$

The method to obtain the coefficients of stress factor models can be found in [18] and is not described in detail in the present paper.

Note that the proposed model structure described in Section II-A can be applied to other batteries, including lithium-iron phosphate and nickel manganese cobalt oxide (NMC) batteries. The degradation processes of these batteries can be divided into three stages. Once the proposed model is applied to different materials, the stress factor models and parameters must be modified. For example, an exponential DOD stress factor model is often used for LFP batteries, and a secondary model is used for NMC batteries.

III. Reliability Assessment and Weak Component Analysis of BES

In general, the reliability of a BES system is not equal to that of a battery cell. Here, we focus on how to measure the reliability of a BES system with differentiated batteries and evaluate the cells that might diminish the reliability.

A. Capacity Probabilistic Modeling and Reliability Evaluation

Accurately measuring the lithium-ion battery capacity during an actual operation is difficult. Therefore, a normal distribution is widely used to describe the probabilistic capacity distribution of lithium-ion batteries. The SOHs calculated using (5) can be used to determine the mean SOH, where the variance can be regarded as a linear relationship with the mean SOH, that is, $\sigma=(1-\mu)/6$ [8]. According to the mean value, the battery SOH can be further grouped into several grades such as 100%-95%, 95%-90%, ..., 25%-20%. To ensure that the sum of the probabilities at each grade is 1, the cumulative distribution function (CDF) of the normal distribution must be adjusted as:

$$F'(x)=\frac{F(x)-F(0)}{F(1)-F(0)} \quad x\in[0,1] \tag{14}$$

Thus, the probability in the j^{th} grade $\left[SOH_j^{\text{low}}, SOH_j^{\text{up}}\right]$ can be obtained as:

$$p_j=F'\left(SOH_j^{\text{up}}\right)-F'\left(SOH_j^{\text{low}}\right) \tag{15}$$

The variance increases as the SOH decreases, and the lower the SOH, the wider the probability distribution, as shown in Fig. 1. Reliability modeling and assessment of the BES are as follows.

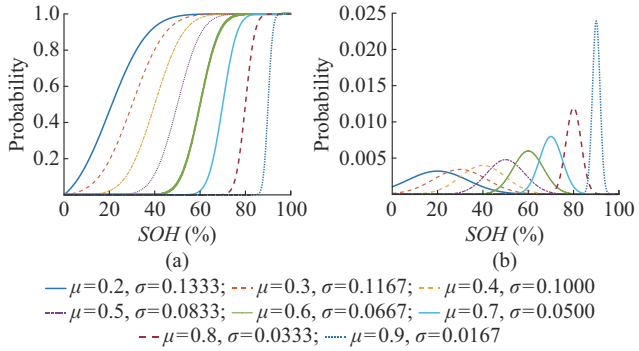

Fig. 1. Different SOH probability distributions as SOH decreases. (a) CDF. (b) PDF.

Step 1: definition and calculation law of UGF.

The UGF of the battery can be expressed as follows. Note that the operator "$\sum$" does not represent algebraic addition but is used only to represent a set.

$$U_{\text{R}}(z)=\sum_{j=1}^{M}p_j z^{G_j} \tag{16}$$

A symbolic multiplier must be defined. Note that this symbol multiplier computation follows commutative and associative methods [9].

$$\Omega\left(U_{\text{R}}^{j_1},U_{\text{R}}^{j_2}\right)=\sum_{j_1=1}^{M}\sum_{j_2=1}^{M}p_{j_1}p_{j_2}z^{f\left(G_{j_1},G_{j_2}\right)} \tag{17}$$

The function f refers to the total SOH of two batteries connected in series and is determined by the worst one in series, whereas the total SOH of two batteries connected in parallel is the average SOH.

$$f\left(G_{j_1},G_{j_2}\right)=\begin{cases}\text{mean}\left(G_{j_1},G_{j_2}\right) & \text{cells in parallel}\\ \min\left(G_{j_1},G_{j_2}\right) & \text{cells in series}\end{cases} \tag{18}$$

Step 2: UGF calculation of BES.

BES is composed of many battery cells in series or parallel combinations. Assuming that the BES includes N_{p} parallel branches with each branch formed by N_{s} cells in series, we can calculate the UGF of a series branch by:

$$U_{\text{serieschain}}(z)=\Omega\left(U_{\text{R}}^{1},U_{\text{R}}^{2},\ldots,U_{\text{R}}^{N_{\text{s}}}\right)=\sum_{j=1}^{M}p_j' z^{G_j} \tag{19}$$

In addition, the final UGF of the BES can be obtained by combining the UGFs of the series branches.

$$U_{\text{BES}}(z)=\Omega\left(U_{\text{serieschain}}^{1},U_{\text{serieschain}}^{2},\ldots,U_{\text{serieschain}}^{N_{\text{p}}}\right)=\sum_{j=1}^{M}p_j'' z^{G_j} \tag{20}$$

Step 3: capacity probability and reliability of BES.

The CDF of the BES can be derived using (20):

$$F_{\text{BES}}(x)=\sum_{j|G_j>x}p_j'' \quad 0\le x\le 1 \tag{21}$$

We can define the reliability of the BES with the required threshold and expected SOH as [8], [9]:

$$\begin{cases}R_{\text{BES}}\{\Psi\}=F_{\text{BES}}(\omega)=\sum_{j|G_j>x}p_j'' & 0\le x\le 1\\ E_{\text{BES}}\{\Psi\}=\sum_{G_j>\omega}p_j''\cdot SOH_{G_j}\end{cases} \tag{22}$$

where ω is typically set to be 80%. Because the proposed aging model is suitable for estimating the battery SOH below 80%, the SOH threshold can be designed to be lower to meet the needs of different scenarios. Note that the BES also includes the power conversion system, battery management system, and other subsystems. This paper focuses on the battery degradation process and the level of system reliability after grouping. The operational reliability analysis of power electronic equipment is provided in a previous paper [36].

B. Reliability Indexes and Weak Component Identification

Following the reliability evaluation, effectively measuring the short-board battery in a BES system is necessary. This paper establishes two types of measurement indexes that consider the current battery state as well as state changes over a short period. An entropy weight method is used to form the reliability importance (RI) index to analyze weak battery cells comprehensively.

1) Establishing State-oriented and State-change-oriented Index Systems for Weak-link Analysis

According to the current states of the battery cells and the BES reliability, this paper proposes the following state-ori-

ented indexes. The first index $I_{\mathrm{SOH},k}=SOH_k$ reflects the SOH of each battery cell. The second index is the reliability probability sensitivity $I_{\mathrm{Rp},k}$, which reflects the effect of the SOH change of the k^{th} battery cell on the change in BES reliability. Its essence is the partial differential of the BES reliability index to the SOH parameter of each battery cell. The third index further considers the current SOH level of the battery cell and the BES reliability. This is because, for battery cells with a high SOH, replacing them with higher-SOH batteries to improve the BES reliability is virtually impossible. Thus, the reliability critical sensitivity $I_{\mathrm{Rc},k}$ is introduced as:

$$\begin{cases} I_{\mathrm{Rp},k}=\dfrac{\partial R_{\mathrm{BES}}}{\partial SOH_k} \\ I_{\mathrm{Rc},k}=\dfrac{\partial R_{\mathrm{BES}}}{\partial SOH_k}\dfrac{SOH_k}{R_{\mathrm{BES}}} \end{cases} \tag{23}$$

Similarly, the fourth index $I_{\mathrm{Ep},k}$ and fifth $I_{\mathrm{Ec},k}$ are the SOH probability sensitivity and SOH critical sensitivity, respectively. These indexes analyze the influence of the battery SOH change on the BES SOH.

$$\begin{cases} I_{\mathrm{Ep},k}=\dfrac{\partial E_{\mathrm{BES}}}{\partial SOH_k} \\ I_{\mathrm{Ec},k}=\dfrac{\partial E_{\mathrm{BES}}}{\partial SOH_k}\dfrac{SOH_k}{E_{\mathrm{BES}}} \end{cases} \tag{24}$$

However, weak-link analysis with only the current cell state cannot effectively consider reliability changes after an operating period. In other words, although some batteries currently have relatively high SOH levels, their reliability might be greatly reduced during the operation. This type of battery cell would not be set as a weak link according to the state-oriented index but would have a greater impact on the overall decrease in reliability. Therefore, this paper further proposes some state-change-oriented indexes as follows.

The first index $I_{\mathrm{dSOH},k}=\Delta SOH_k$ is the SOH change during an operating period. The second index is the reliability contribution index $I_{\mathrm{Rcon},k}$. Its essence is to reflect the percentage of change in BES reliability caused by the SOH change of the k^{th} battery cell during this operating period. And $\Gamma\left(\Delta SOH_k \middle| \Psi(SOH)\right)$ refers to the battery SOH set if the k^{th} battery SOH is increased by ΔSOH_k.

$$I_{\mathrm{Rcon},k}=\frac{\Delta R_{\mathrm{BES}}\left(\Gamma\left(\Delta SOH_k \middle| \Psi(SOH)\right)\right)}{\Delta R_{\mathrm{BES}}} \tag{25}$$

The third index $I_{\mathrm{Econ},k}$ is the degree of change of BES-expected SOH caused by the SOH change of the k^{th} battery cell during this operating time.

$$I_{\mathrm{Econ},k}=\frac{\Delta E_{\mathrm{BES}}\left(\Gamma\left(\Delta SOH_k \middle| \Psi(SOH)\right)\right)}{\Delta E_{\mathrm{BES}}} \tag{26}$$

2) Weak Battery Cell Identification Through Entropy Method

Because the measurement standards of the aforementioned indexes are different, the order of weak battery cells evaluated by different indicators might conflict. Therefore, this paper adopts an entropy weight method to establish the RI index. This index could be used to identify comprehensively weak links that combine both state-oriented and state-change-oriented indexes. The specified algorithm (algorithm 1) is as follows.

Algorithm 1: RI index calculation by entropy weight method

Data input: state-oriented or state-change-oriented indexes of different battery cells. Note that I_k^m represents the m^{th} index value of the k^{th} cell
Output: reliability important indexes of different battery cells

Standardization of different indexes
If the m^{th} index is a positive index, **then**
1.1: Calculate the normalized index as follows. The higher the positive index, the better the battery such as *SOH*

$$I'_{k,m}=\frac{I_k^m-\min\left\{I_1^m,\ldots,I_k^m,\ldots\right\}}{\max\left\{I_1^m,\ldots,I_k^m,\ldots\right\}-\min\left\{I_1^m,\ldots,I_k^m,\ldots\right\}}$$

else if the m^{th} index is negative
1.2: calculate the normalized index as follows. The lower the negative index, the better the battery, such as ΔSOH

$$I'_{k,m}=\frac{\max\left\{I_1^m,\ldots,I_k^m,\ldots\right\}-I_k^m}{\max\left\{I_1^m,\ldots,I_k^m,\ldots\right\}-\min\left\{I_1^m,\ldots,I_k^m,\ldots\right\}}$$

End

Calculate the weight of each index
2.1: calculate the proportion of the k^{th} cell in the m^{th} index ζ_k^m in this index as well as the entropy of the m^{th} index e_m

$$\zeta_k^m=\frac{I'_{k,m}}{\sum_k I'_{k,m}},\quad e_m=-\frac{1}{\ln\left(N_sN_p\right)}\sum_k \zeta_k^m\ln\left(\zeta_k^m\right)$$

2.2: calculate the Laplace distance $dis_m=1-e_m$
2.3: calculate the information entropy redundancy $w_m=\dfrac{dis_m}{\sum_m dis_m}$

Calculate the RI index
3.1: $RI_k=\sum_{m=1}^{M} w_m I'_{k,m}$, where the lower the value, the lower the reliability level, which is a weak link that must be a focal issue

IV. Overview of Operational Reliability Assessment Algorithms

In this section, we briefly explain the structure of the operational reliability assessment algorithm, showing how the reliability of the BES is evaluated step by step. The proposed algorithm evaluates the BES reliability considering the operating conditions and health status of the battery cells. The algorithm overview for evaluating operational reliability of BES is illustrated in Fig. 2.

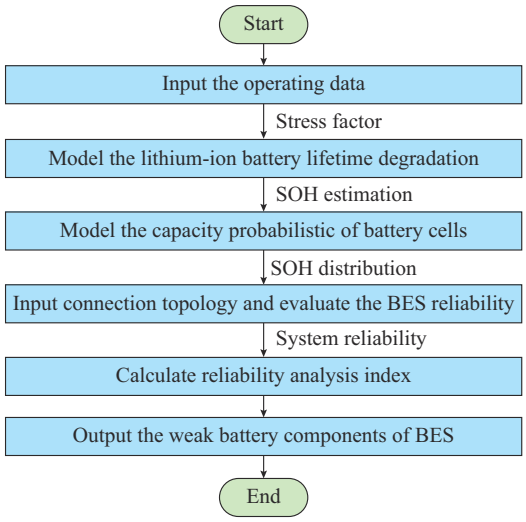

Fig. 2. Algorithm overview for evaluating operational reliability of BES.

Above all, the assessment basis is to establish a condition-dependent reliability model to reflect the relationship between the lithium-ion battery life and shelving time, DOD, SOC, and battery temperature. Based on the evaluation of the battery cell life, the core of the reliability assessment is to analyze the variation in the degree of BES reliability with a specific topology connection in a short term. Reliability indexes are then established to guide weak-link identification. These works are meaningful for realizing reliability optimization and redundant backup design of BES systems.

In contrast to the test data of cycle aging, the average SOC, DOD, number of cycles, and other parameters required for evaluation are often irregular in actual operation. Fortunately, the rainflow cycle-counting algorithm is widely used in calculating fatigue life and can be adapted for effectively calculating the stress effect. The specific calculation rules of the rainflow algorithm can be found in [37]. This paper uses the SOC profile as the algorithm input, and the following information can be obtained: the DOD of each cycle, average SOC of each cycle, number of cycles (0.5 for a half cycle, or 1 for a full cycle), start and end time of the cycle, and cycle duration. The average temperature of each cycle can be obtained by combining the temperature profile and the start and end time of the cycle.

V. Case Studies

Initially, we need to examine the validity of the proposed lifetime degradation model of lithium-ion battery, including the rationality and accuracy of the proposed parameters for evaluating the SEI formation point of and capacity plummeting point. The second objective is to illustrate the proposed reliability assessment algorithm and analyze the effects of different changing conditions on reliability performance of the BES.

A. Verification of Lifetime Degradation Model for Lithium-ion Batteries

Most battery degradation models are suitable only for the remaining life analysis of batteries with capacities greater than 80% [8], [14], [18]. Once these models are applied to the evaluation of decommissioned batteries, the results might be relatively optimistic when neglecting the phenomenon of battery capacity plummeting.

This subsection describes the use of aging test data provided by the Battery Research Group of the Center for Advanced Life Cycle Engineering to verify the validity of the proposed lifetime degradation model [38]. A $LiCoO_2$ battery is used in the experiments. For the charging stage, each battery is charged at a constant current of 0.5 until the voltage reaches 4.2 V, and then 4.2 V is sustained until the charging current drops below 0.05 A. The discharging conditions of each battery are different, and a label of "CS2_n" is assigned to the n^{th} numbered CS2 cell. The fitting results of the proposed model are presented based on the cyclic data, and the rationalities for the setting of the SEI formation point α_{sei} and the capacity plummeting point $\alpha_{sei}+\alpha_{sds}$ are explained. The performance of the model under different working conditions is further demonstrated.

1) Model Verification Utilizing Aging Test Data

The batteries numbered from CS2-35 to CS2-38 are discharged at a constant current of 1 until the voltage drops to 2.7 V. Continuous complete charging and discharging cycles are performed in this mode until the SOH drops to approximately 15%. The fitting results for battery CS2-35 are shown in Fig. 3.

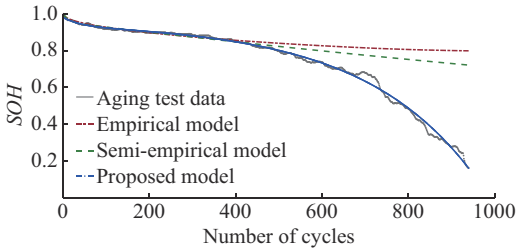

Fig. 3. Fitting results for battery CS2-35.

The parameters of the traditional empirical [14] and semi-empirical [18] models are identified using SOH data greater than 80%. However, these models cannot reflect the phenomenon of capacity plummeting, whereas the proposed model can be well fitted to 20% SOH data.

In addition, this paper adopts the root mean square error (RMSE) and R-squared value (R2) for a quantitative analysis of the fitting effect. RMSE and R2 values of different models with different models are shown in Fig. 4. When the fitting results of the degradation data greater than 80% SOH are compared, the fitting accuracy of the proposed model is close to that of the semi-empirical model in [18]. The corresponding fitting indicators RMSE and R2 are basically in an intermediate position between the empirical and traditional semi-empirical models. The proposed model also exhibits a good fitting effect for the data greater than 20% SOH. The R2 value is greater than 99%.

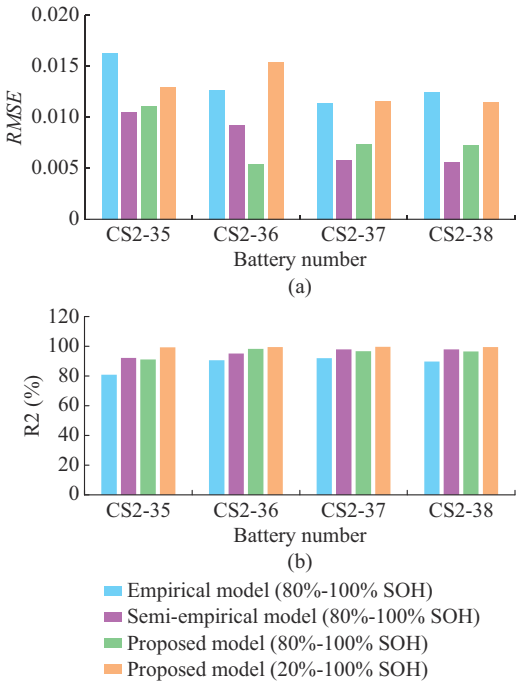

Fig. 4. RMSE and R2 values of different models with different models. (a) RMSE. (b) R2.

2) Parameter Rationality of SEI Formation Point and Capacity Plummeting Point

As shown in Fig. 4, the semi-empirical model compared in this paper could identify the SEI formation point (α_{sei} = 8.39%) by the degradation data above 80% SOH, whereas the SEI formation point and capacity plummeting point could be identified through the proposed model, i.e., α_{sei} = 9.98% and $\alpha_{sei}+\alpha_{sds}$ = 16.32%. When capacity plummeting occurs, i.e., where the degradation curve is convex, and the threshold value is not 80% but 83.68%. However, the semi-empirical model cannot fit a convex curve. Therefore, for a battery with a capacity plummeting point greater than 80% SOH, the fitting results would be worse if the degradation data above 80% SOH are used. We could then utilize the plummeting point in the proposed model to further define the applicable range of the compared semi-empirical model, as shown in Fig. 5.

The parameters of the proposed and comparison models are listed in Table I. These models have similar identification results for the SEI formation point. After the proposed plummeting point is used to modify the applicable range of the comparison model to a suitable degree, the fitting effect of the comparison model is also improved to a certain extent. In addition, the SEI formation point values are closer when the semi-empirical model and the proposed model are used, which further verifies the rationality of the parameters of our model.

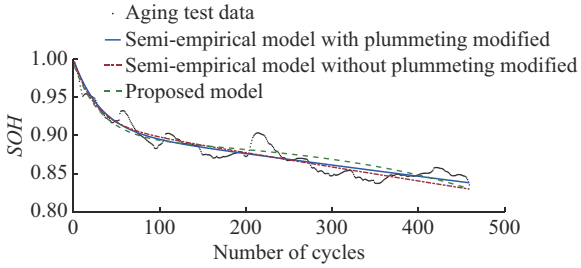

Fig. 5. Applicable range of compared semi-empirical model.

TABLE I
PARAMETER COMPARISONS OF DIFFERENT MODELS

Model	CS2-35				CS2-36				CS2-37			
	RMSE	R2 (%)	α_{sei} (%)	$\alpha_{sei}+\alpha_{sds}$ (%)	RMSE	R2 (%)	α_{sei} (%)	$\alpha_{sei}+\alpha_{sds}$ (%)	RMSE	R2 (%)	α_{sei} (%)	$\alpha_{sei}+\alpha_{sds}$ (%)
Semi-empirical model without plummeting modified	0.0105	92.18	8.39		0.0092	95.08	4.41		0.0058	97.90	7.94	
Semi-empirical model with plummeting modified	0.0099	92.76	9.33		0.0051	97.09	5.10		0.0059	97.58	8.03	
Proposed model	0.0130	99.36	9.98	16.32	0.0154	99.44	4.93	15.35	0.0116	99.44	9.21	18.76

3) Case 3: Analysis of Parameter Sensitivity

Battery degradation is affected by various factors. In this paper, the CS2-5 battery is cycled in a low-regime partial charging/discharging cycle (5%-70%), and the CS2-25 battery is cycled in a high-regime partial charging/discharging cycle (70%-100%). These data could be used to analyze the relationship between the change in the degradation profile and the average SOC level. In addition, the CS2-7 battery is cycled at a constant current discharge, whereas the cut-off voltage is changed at random times to simulate different DOD conditions. The capacity degradation process under different conditions is shown in Fig. 6. The movements of the profiles also indicate that the proposed model could accurately reflect the effects of different operating conditions on battery aging.

B. Application of Degradation Model

It should be noted that the aforementioned verification of the degradation model is mainly based on the cycle aging test data. It can be assumed that the working conditions of each cycle are basically the same, which means that the degradation rate in the stable degradation stage is a fixed value. This rate can be directly identified as a fitting parameter. However, in actual operation, the degradation rate $d_{sds}(t,\tau,v,T)$ is a changing value determined by the operating conditions, which mainly includes the calendar aging rate $d_t(t,\bar{\tau},\bar{T})$ and cycle aging rate $d_c(\tau_i,v_i,T_i)$.

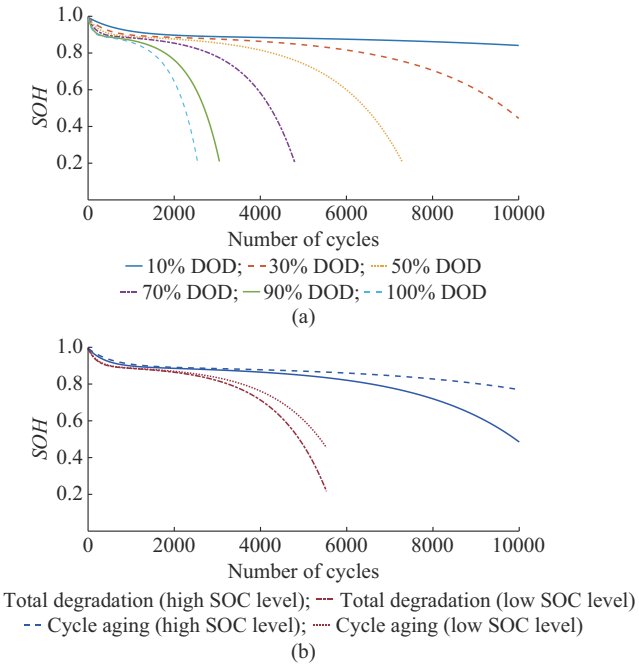

Fig. 6. Capacity degradation process under different conditions. (a) Degradation process for different DODs. (b) Degradation process at different SOC levels.

This subsection describes the use of actual operating data of an EV to further explain the proposed model. Figure 7 shows the actual operational data for SOC profile of an EV over half a year.

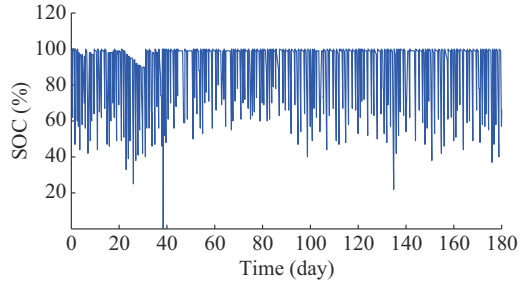

Fig. 7. Actual operational data for SOC profile of an EV over half a year.

The cycle distribution of SOC profile is shown in Fig. 8. The figure shows the average SOC, DOD, and corresponding number of cycles. The effective cycle DOD is mainly concentrated between 20% and 80%, and the corresponding average SOC is between 50% and 80%.

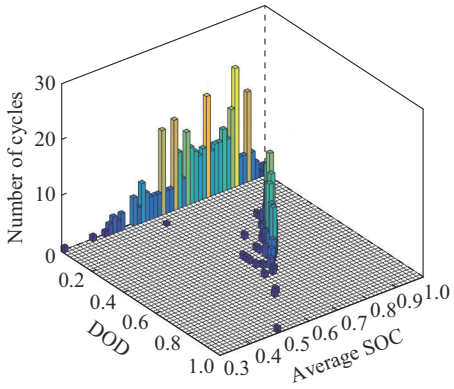

Fig. 8. Cycle distribution of SOC profile.

The results of the rainflow method could be substituted into the corresponding stress factor models, as described in Section II-B. The daily degradation rate, including the total degradation rate and the calendar and cycle aging rates, could be obtained, as shown in Fig. 9. The parameters used in the stress and aging models can be found in Appendix A. It can be observed that the daily aging rate varies with the daily operating conditions (different SOC curve inputs). Among these, a rate spike occurred on the 39th day. This was because the DOD value on this day reached 100%, causing the cycle aging rate to far exceed the average. Continual operation in this mode reveals the degradation process of the battery, as shown in Fig. 10. The traditional semi-empirical model causes a significant prediction error after 2000 days of operation, which cannot reflect the phenomenon of battery capacity plummeting. The batteries can continue to be in service for approximately 1200 days below 80% SOH. This means that decommissioned bus batteries or UPS decommissioned batteries of the data center still have a certain amount of space for reuse. In these applications, the price of secondary batteries is 30%-70% cheaper than that of new batteries, which can effectively improve the economic benefits of the BES system.

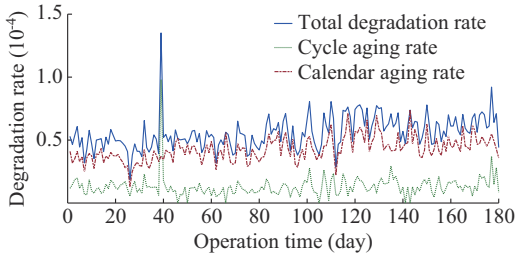

Fig. 9. Daily degradation rates under different conditions.

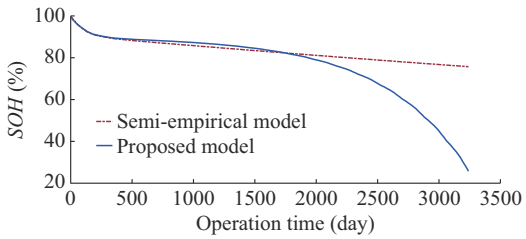

Fig. 10. Degradation process of battery.

C. BES Reliability

The probability distribution of the cell capacity could be obtained based on the battery capacity degradation process shown in Fig. 10. Assuming that a certain energy storage system is composed of $2^8 \times 2^2$ battery cells and that the battery consistency is at a high level, we could calculate the reliability level and expected capacity of the BES. The difference between the expected BES capacity and expected cell capacity increases with decreasing expected cell SOH, as shown in Fig. 11. When the battery SOH is approximately 30%, the expected BES capacity is only approximately 10%.

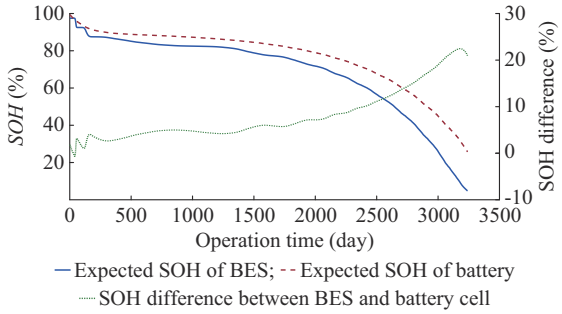

Fig. 11. Expected SOHs of BES and battery cell.

In addition, Fig. 12 shows the changes in reliability when different thresholds are set. If 90% SOH is set as the evaluation reference, the system reliability would drop rapidly in approximately 210 days. When $w = 80\%$, the reliability would decrease by approximately 1000 days, and the system can still operate for approximately 450 days until the probability of the expected capacity falling below the threshold w is greater than 50%. However, when the threshold is set too high or low, the slope of the reliability profile increases. This is because when the threshold is in the SEI formation and capacity plummeting stages, the battery degradation rate is relatively high. The shorter cycle period may have also caused a large SOH change, resulting in a faster decline in reliability.

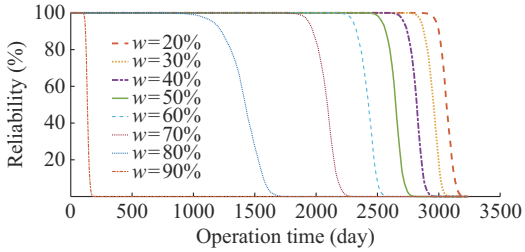

Fig. 12. Reliability profiles under different threshold settings.

This paper selects 60%, 70%, and 80% as the thresholds to compare the reliability difference between the proposed model and the model in [18], as shown in Fig. 13. After considering the capacity plummeting, the reliability profiles of the BES are also found to be different. Taking the 80% threshold as an example, the BES reliability of the proposed model is above 80% within 1000 days of operation. The result of the comparison model is 1300 days, and the reliability evaluation result is relatively optimistic.

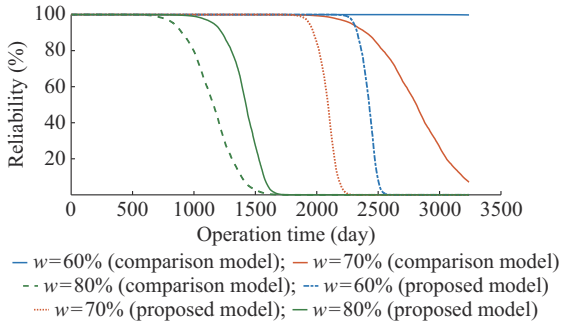

Fig. 13. BES reliability profiles based on different aging models.

D. Application of Reliability Assessment and Weak Component Analysis

The degradation parameters and initial SOHs of the battery cells as described in Section V-C are changed to different values. The reliability level of the BES composed of differentiated batteries in the short-term operation is further analyzed. The index system constructed as described in Section II-B is used to identify weak links. With the initial capacities of the battery assumed to be random values of [78%, 82%], the parameters α_{sei}, β_{sei}, α_{sds}, β_{cps}, and κ are the random values of the intervals [4%, 8%], [100, 150], [11%, 17%], [25, 30], and [0.005,0.01], respectively. The threshold value w is 70%. With different model parameters, the battery degradation processes are also different under the same working conditions. Because the capacity of the battery does not change significantly in a short term, it can be assumed that the SOC changes of each battery in the short term are consistent (obtained from 110 to 140 days in Fig. 7). Figure 14 illustrates the variations in the BES reliability composed of consistent batteries and differentiated cells. After 30 days of operation, the BES reliability composed of differentiated batteries decreases more than that of the BES composed of the same batteries. The BES probability distributions presented in Fig. 15 show that the SOH has an obvious left deviation, and the most likely grade has changed from [71%, 72%] to [70%, 71%].

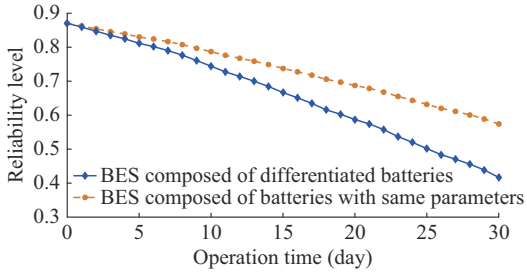

Fig. 14. Reliability variations in BES composed of differentiated batteries and batteries with same parameters.

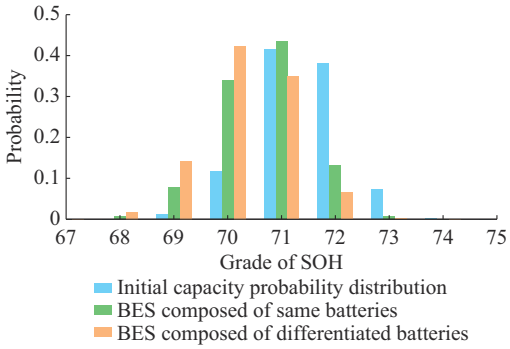

Fig. 15. Comparison of BES probability distributions.

As shown in Table II, various indexes can be further used to search for the weak links of the BES, and the batteries with the greatest reliability impact obtained by different indexes are also different. The worst battery searched by the index $I_{SOH.\,k}$ is N(3,174), the *SOH* of which is 77.07%. The battery with the largest ΔSOH is N(1,31), which changes by 0.9884%. The worst battery obtained using the other indexes is N(4,196). Based on the evaluation results of the state-oriented and state-change-oriented indexes, the worst 20 battery rankings could be obtained using the RI index. The batteries also differ in terms of the order of weakness when evaluated using other single indexes, as shown in Fig. 16.

TABLE II
WORST BATTERY NUMBERS AND CORRESPONDING INDEX VALUES BY DIFFERENT INDEXES

Worst battery	I_{Rp} (%)	I_{Ep} (%)	I_{Rcon} (%)	I_{Econ} (%)	I_{SOH} (%)	I_{dSOH} (%)
N(4,196)	0.243	0.005	0.398	0.350		
N(3,174)					77.066	
N(1,31)						0.988

For instance, the N(2,142) battery is the ninth-worst battery based on the RI index. However, when the reliability contribution index I_{Rcon}, SOH change index I_{dSOH}, reliability sensitivity index I_{Rp}, and SOH are considered, the battery ranks 12th, 42nd, 16th, and 3rd, respectively. As another example, the N(3,159) battery ranks only 112nd based on the SOH change index and is hardly a weak link, but its ranking is 7th based on the analysis of various sensitivities and contribution indexes. This also indicates that the use of the RI index proposed in this paper could more comprehensively consider the effects of changes in battery status and operating status

and could be used to generate the evaluations of weak links more accurately.

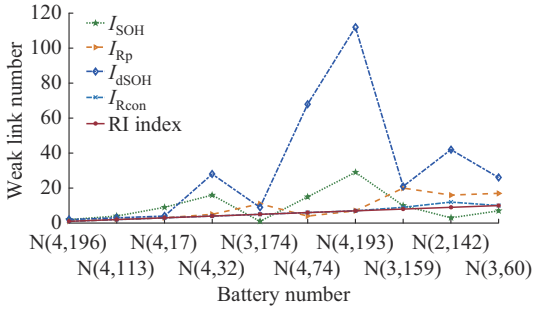

Fig. 16. Rankings of weaknesses as measured by different indexes.

VI. Conclusion

By considering the effects of different conditions and component aging status, this paper proposes a reliability modeling and evaluation algorithm for BES systems based on lithium-ion battery lifetime degradation. RIs and weak-link identification methods are developed for reliability evaluation of BESs with differentiated cells. The following conclusions can be drawn from the case studies.

1) A semi-empirical lifetime degradation model can reflect the degradation process of lithium-ion batteries before the key parameters proposed by the model can fully reflect the SEI formation point (upward convex part) and the capacity plummeting point (downward convex part), which can be identified based on the key parameters proposed by the model. In addition, this model can reflect the effects of different working conditions on the degradation rate. It is worth noting that these parameters can also be used to improve the fitting accuracy of some models that apply only to new batteries.

2) When the probability distribution of the battery capacity is modeled using the UGF method, a reliability assessment of the BES could be realized. The threshold value can be extended from 80% SOH to 20% SOH by considering the conditions of the entire life degradation process. Results of the numerical examples further demonstrate that the reliability analytical results obtained by the proposed method are reasonable. In addition, the reliability decline rate of BESs with different battery compositions is also greater due to different levels of battery health and different aging rates.

3) State-oriented and state-change-oriented indexes are developed to analyze the effects of battery cells on the overall BES reliability. Because the emphasis of each index is different, the case studies show that conflicting results may occurr in analyzing the weak links through these indexes. A comprehensive evaluation RI index for reliability weak links can fully consider the effects of various indexes, and the rankings of weak links provide greater insights into BES design and operation.

It should be noted that the parameters of battery lifetime degradation can be obtained only through aging experimental data. The method used in this paper can be effectively incorporated into the economic calculation of the BES cost. However, for a battery under real-time operation, the data-driven online identification method of degradation parameters needs to be further studied in the future. In addition, considering the effects of weak links, we plan to focus on the optimal operation of BES systems by using reconfigurable battery network technology to isolate weak batteries or to reconstruct the topologies.

Appendix A

The parameters of the degradation model and stress factor models could be found in the Table AI.

TABLE AI
Parameters of Degradation Model

Model	Parameter	Value
Lifetime degradation model	α_{sei}	0.0998
	α_{sds}	0.0634
	β_{sei}	154.2382
	β_{cps}	26.1116
	κ	0.0068
DOD stress factor model	$k_{\upsilon 1}$	1.4×10^{5}
	$k_{\upsilon 2}$	-5.01×10^{-1}
	$k_{\upsilon 3}$	-1.23×10^{5}
SOC stress factor model	k_{τ}	1.04
	τ_{ref}	0.5
Time stress factor model	k_t	$4.14\times10^{-10}/s^{-1}$
Temperature stress factor model	k_T	6.93×10^{-3}
	T_{ref}	25 ℃

References

[1] E. Pusceddu, B. Zakeri, and G. C. Gissey, "Synergies between energy arbitrage and fast frequency response for battery energy storage systems," *Applied Energy*, vol. 283, no. 116274, pp. 1-17, Feb. 2021.
[2] K. Wang, Y. Qiao, L. Xie *et al*., "A fuzzy hierarchical strategy for improving frequency regulation of battery energy storage system," *Journal of Modern Power Systems and Clean Energy*, vol. 9, no. 4, pp. 689-698, Jul. 2021.
[3] D. M. Davies, M. G. Verde, O. Mnyshenko *et al*., "Combined economic and technological evaluation of battery energy storage for grid applications," *Nature Energy*, vol. 4, pp. 42-50, Aug. 2019.
[4] A. Bhatt, S. Tiwari, and W. Ongsakul, "A review on re-utilization of electric vehicle's retired batteries," in *Proceedings of 2018 International Conference and Utility Exhibition on Green Energy for Sustainable Development*, Phuket, Thailand, Oct. 2018, pp. 1-5.
[5] Y. Deng, Y. Zhang, F. Luo *et al*., "Operational planning of centralized charging stations utilizing second-life battery energy storage systems," *IEEE Transactions on Sustainable Energy*, vol. 12, no. 1, pp. 387-399, Jan. 2021.
[6] Y. Chen, Y. Zheng, F. Luo *et al*., "Reliability evaluation of distribution systems with mobile energy storage systems," *IET Renewable Power Generation*, vol. 10, no. 10, pp. 1562-1569, Jun. 2016.
[7] T. T. Pham, T. C. Kuo, D. M. Bui *et al*., "Impact of dynamic operation on reliability of an aggregate battery energy storage system," in *Proceedings of 2019 IEEE PES Asia-Pacific Power and Energy Engineering Conference*, Macao, China, Dec. 2019, pp. 1-6.
[8] Q. Xia, Z. Wang, Y. Ren *et al*., "A modified reliability model for lithium-ion battery packs based on the stochastic capacity degradation and dynamic response impedance," *Journal of Power Sources*, vol. 423, pp. 40-51, Mar. 2019.
[9] M. Liu, W. Li, C. Wang *et al*., "Reliability evaluation of large scale battery energy storage systems," *IEEE Transactions on Smart Grid*, vol. 8, no. 6, pp. 2733-2743, Nov. 2017.
[10] Q. Xia, Z. Wang, Y. Ren *et al*., "A reliability design method for a lithium-ion battery pack considering the thermal disequilibrium in electric vehicles," *Journal of Power Sources*, vol. 386, pp. 10-20, Mar. 2018.
[11] L. Zhang, Z. Mu, and C. Sun, "Remaining useful life prediction for

lithium-ion batteries based on exponential model and particle filter," *IEEE Access*, vol. 6, pp. 17729-17740, Mar. 2018.
[12] Y. B. Liaw, R. Jungst, G. Nagasubramanian *et al*., "Modeling capacity fade in lithium-ion cells," *Journal of Power Sources*, vol. 140, no. 1, pp. 157-161, Jan. 2005.
[13] D. Ouyang, M. Chen, J. Weng *et al*., "A comparative study on the degradation behaviors of overcharged lithium-ion batteries under different ambient temperatures," *International Journal of Energy Research*, vol. 44, no. 2, pp. 1078-1088, Mar. 2020.
[14] J. Schmalstieg, S. Käbitz, M. Ecker *et al*., "A holistic aging model for Li(NiMnCo)O_2 based 18650 lithium-ion batteries," *Journal of Power Sources*, vol. 257, pp. 325-334, Jul. 2014.
[15] X. Li, J. Jiang, L. Wang *et al*., "Capacity model based on charging process for state of health estimation of lithium ion batteries," *Applied Energy*, vol. 177, pp. 537-543, Sept. 2016.
[16] Q. Zhang and E. R. White, "Capacity fade analysis of a lithium ion cell," *Journal of Power Sources*, vol. 179, no. 2, pp. 793-798, May 2008.
[17] I. Laresgoiti, S. Käbitz, M. Ecker *et al*., "Modeling mechanical degradation in lithium ion batteries during cycling: solid electrolyte interphase fracture," *Journal of Power Sources*, vol. 300, pp. 112-122, Dec. 2015.
[18] B. Xu, A. Oudalov, A. Ulbig *et al*., "Modeling of lithium-ion battery degradation for cell life assessment," *IEEE Transactions on Smart Grid*, vol. 9, no. 2, pp. 1131-1140, Mar. 2018.
[19] Q. Hou, Y. Yu, E. Du *et al*., "Embedding scrapping criterion and degradation model in optimal operation of peak-shaving lithium-ion battery energy storage," *Applied Energy*, vol. 278, no. 115601, pp. 1-9, Aug. 278.
[20] K. Takei, K. Kumai, Y. Kobayashi *et al*., "Cycle life estimation of lithium secondary battery by extrapolation method and accelerated aging test," *Journal of Power Sources*, vol. 97-98, pp. 697-701, Jul. 2001.
[21] M. Förstl, D. Azuatalam, A. Chapman *et al*., "Assessment of residential battery storage systems and operation strategies considering battery aging," *International Journal of Energy Research*, vol. 44, no. 2, pp. 718-731, Feb. 2020.
[22] X. Chen, J. Tang, W. Li *et al*., "Operational reliability and economy evaluation of reusing retired batteries in composite power systems," *International Journal of Energy Research*, vol. 44, no. 5, pp. 3657-3673, Jan. 2020.
[23] L. Yang, X. Cheng, Y. Gao *et al*., "Lithium deposition on graphite anode during long-term cycles and the effect on capacity loss," *RSC Advances*, vol. 4, pp. 26335-26341, May 2014.
[24] M. Ecker, S. P. Sabet, and D. U. Sauer, "Influence of operational condition on lithium plating for commercial lithium-ion batteries-electrochemical experiments and post-mortem-analysis," *Applied Energy*, vol. 206, pp. 934-946, Sept. 2017.
[25] K. Brik and F. B. Ammar, "The fault tree analysis of the lead acid battery's degradation," *Journal of Electrical System*, vol. 4, no. 2, pp. 145-159, Jun. 2008.
[26] E. Chatzinikolaou and D. J. Rogers, "A comparison of grid-connected battery energy storage system designs," *IEEE Transactions on Power Electronics*, vol. 32, no. 9, pp. 6913-6923, Sept. 2017.
[27] Y. Lin, M. Hu, X. Yin *et al*., "Evaluation of lithium batteries based on continuous hidden Markov model," in *Proceedings of 2017 IEEE International Conference on Software Quality, Reliability and Security Companion*, Prague, Czech, Jul. 2017, pp. 221-225.
[28] B. Scrosati and J. Garche, "Lithium batteries: status, prospects and future," *Journal of Power Sources*, vol. 195, no. 9, pp. 2419-2430, May 2010
[29] Z. Liu, C. Tan, and F. Leng, "A reliability-based design concept for lithium-ion battery pack in electric vehicles," *Reliability Engineering & System Safety*, vol. 134, pp. 169-177, Feb. 2015.
[30] R. Spotnitz, "Simulation of capacity fade in lithium-ion batteries," *Journal of Power Sources*, vol. 113, no. 1, pp. 72-80, Jan. 2003.
[31] M. Mureddu, A. Facchini, A. Damiano *et al*., "A statistical approach for modeling the aging effects in li-ion energy storage systems," *IEEE Access*, vol. 6, pp. 42196-42206, Jul. 2018.
[32] A. Millner, "Modeling lithium ion battery degradation in electric vehicles," in *Proceedings of 2010 IEEE Conference on Innovative Technologies for an Efficient and Reliable Electricity Supply*, Waltham, USA, Sept. 2010, pp. 349-356.
[33] I. Laresgoiti, S. Käbitz, M. Ecker *et al*., "Modeling mechanical degradation in lithium ion batteries during cycling: solid electrolyte interphase fracture," *Journal of Power Sources*, vol. 300, pp. 112-122, Dec. 2015.
[34] X. Han, M. Ouyang, and L. Lu, "A comparative study of commercial lithium ion battery cycle life in electrical vehicle: aging mechanism identification," *Journal of Power Sources*, vol. 251, pp. 38-54, Apr. 2014.
[35] B. Y. Liaw, E. P. Roth, R. G. Jungst *et al*., "Correlation of arrhenius behaviors in power and capacity fades with cell impedance and heat generation in cylindrical lithium-ion cells," *Journal of Power Sources*, vol. 119-121, pp. 874-886, Jun. 2003.
[36] Y. Wan, L. Cheng, and M. Liu, "Operational reliability assessment of power electronic transformer considering operating conditions and fatigue accumulation," in *Proceedings of 2020 International Conference on Probabilistic Methods Applied to Power Systems*, Liege, Belgium, Aug. 2020, pp. 1-6.
[37] P. P. Mishra, A. Latif, M. Emmanuel *et al*., "Analysis of degradation in residential battery energy storage systems for rate-based use-cases," *Applied Energy*, vol. 264, no. 114632, pp. 1-17, Feb. 2020.
[38] Battery Research Group of the Center for Advanced Life Cycle Engineering. (2021, Jan.). [Online]. Available: https://web. calce. umd. edu/batteries/data.htm#

Lin Cheng received the B.S. degree in electrical engineering from Tianjin University, Tianjin, China, in 1996, and the Ph.D. degree in electrical engineering from Tsinghua University, Beijing, China, in 2001. Currently, he is a Tenured Professor with the State Key Laboratory of Power Systems, Department of Electrical Engineering, Tsinghua University. His research interests include operational reliability evaluation and application of power systems, synchronized measurement application in power systems, battery energy storage system modeling and operation.

Yuxiang Wan received the B.S. degree in electrical engineering from Tsinghua University, Beijing, China, in 2017. Currently, he is pursuing a Ph.D. degree at the State Key Laboratory of Power Systems, Tsinghua University. His research interests include battery energy storage system reliability assessment, power system reliability analysis and demand response.

Yanglin Zhou received the Ph.D. degree from the University of Chinese Academy of Sciences, Beijing, China, in 2020. Currently, he is a Postdoctoral Researcher with the Department of Electrical and Engineering, Tsinghua University, Beijing, China. His research interests include control strategy of battery energy storage system, demand response in smart grid, peer to peer energy sharing in energy internet.

David Wenzhong Gao received the M.S. and Ph.D. degrees in electrical and computer engineering, specializing in electric power engineering, from the Georgia Institute of Technology, Atlanta, USA, in 1999 and 2002, respectively. He is a Tenured Professor with the Department of Electrical and Computer Engineering, University of Denver, Denver, USA. His current teaching and research interests include renewable energy and distributed generation, microgrids, smart grids, power system protection, power electronic applications, power system modeling and simulation, and hybrid-electric propulsion systems.